

Lawrence Berkeley National Laboratory

LBL Publications

Title

Structure and Orientation of Molecular Wires Embedded in Ultrathin Silica Membrane for Artificial Photosynthesis Elucidated by Polarized FT-IRRAS

Permalink

<https://escholarship.org/uc/item/462769km>

Journal

The Journal of Physical Chemistry C, 123(31)

ISSN

1932-7447

Authors

Katsoukis, Georgios
Jo, Won Jun
Frei, Heinz

Publication Date

2019-08-08

DOI

10.1021/acs.jpcc.9b02523

Peer reviewed

**Structure and Orientation of Molecular Wires Embedded in Ultrathin
Silica Membrane for Artificial Photosynthesis Elucidated by
Polarized FT-IRRAS**

Georgios Katsoukis, Won Jun Jo, and Heinz Frei*

Molecular Biophysics and Integrated Bioimaging Division, Lawrence Berkeley
National Laboratory, University of California, Berkeley, CA 94720

HMFrei@lbl.gov

Abstract

Surface sensitive infrared spectroscopic methods are employed for elucidating the structure and orientation of charge conducting molecular wires of type oligo *p*-(phenylene vinylene) covalently anchored on an ultrathin planar Co oxide catalyst surface and embedded in a few nanometer thick amorphous silica membrane. Comparison of polarized FT-IRRAS with non-polarized grazing angle ATR FT-IR spectra of nanolayer samples supported on a flat Pt surface and transmission spectra of powder samples showed distinct intensity differences for molecular in-plane and out-of-plane modes that reveal the spatial orientation with respect to the oxide surface. All observations support an upright orientation of the molecular wire axis, which is further confirmed by comparison with IRRAS measurements of physisorbed, horizontally positioned wire molecules. Structural integrity of the molecules is maintained after embedding in silica membrane by plasma-enhanced atomic layer deposition at 40°C. The results provide the first spectroscopic evidence of perpendicular orientation of the wire molecules. The complementary surface sensitive infrared measurements by FT-IRRAS and grazing angle FT-IR constitute a powerful approach for elucidating the structure and orientation of surface anchored molecules, and the integrity upon casting into oxide layers such as silica for developing artificial photosystems. Use of the nanolayer construct in IRRAS spectroelectrochemical cell configuration will enable in-situ monitoring of the structural and orientation integrity of the silica embedded molecular wires

under the sustained electron and proton flux conditions of photocatalytic operation.

1. Introduction

Closing of the photosynthetic cycle of carbon dioxide reduction by water on the shortest possible length scale, the nanoscale, for generating solar fuels allows avoiding large energy losses caused by resistance of ion transport over macroscale distances and minimizing efficiency-degrading processes, in particular back or side reactions. Nanoscale integration of H₂O oxidation and CO₂ reduction catalysis requires separation of these incompatible catalysis environments by an ultrathin proton conducting, O₂ impermeable membrane that affords at the same time tightly controlled charge transport across the physical barrier. We are developing macroscale arrays of cobalt oxide – silica core-shell nanotubes designed in a manner that separates the spaces of H₂O oxidation from light absorber and CO₂ reduction environments at all length scales from nano to macro. Each core-shell nanotube is designed to operate as an independent photosynthetic unit for CO₂ photoreduction by H₂O.¹

A novel ingredient, and essential component, of the core-shell nanotube is a 2 nm thick amorphous silica layer with embedded oligo *p*-(phenylene vinylene) molecules (3 aryl units) that provide molecularly defined conduits for tightly controlled charge transfer across the insulating membrane. Methods for anchoring of molecular wires on the Co₃O₄ catalyst surface and establishment of their structural integrity upon casting into silica by solvothermal or atomic layer deposition methods have been pursued with planar, spherical, and nanotube geometry using FT-IR, FT-Raman, XPS, and optical spectroscopy for structural characterization.²⁻⁶ Charge transport

through embedded wires and tight control by their orbital energetics was demonstrated by visible light photoelectrochemical measurements in short circuit configuration.⁴ Transient optical absorption spectroscopy revealed sub ps hole injection from light absorber into embedded wires followed by transfer to Co_3O_4 catalyst within 250 ps.⁷ Proton conductivity across the 2 nm silica membrane was quantified by electrochemical impedance spectroscopy and found to exceed the flux needed under maximum solar intensity by three orders of magnitude, and cyclic voltammetry confirmed that the silica nanolayer completely blocks O_2 from crossing the membrane.⁸

While visible light driven electrochemical and transient optical monitoring of charge transport demonstrates that a substantial fraction of embedded wire molecules span the silica nanolayer so as to function as charge conduits,³⁻⁶ experimental information on the orientation of anchored wires is lacking. Here, we report an infrared spectroscopic study of wire molecules anchored on planar Co_3O_4 and embedded in ultrathin silica layers by polarized Fourier transform-infrared reflection-absorption spectroscopy (FT-IRRAS) and non-polarized grazing angle attenuated total reflection Fourier transform-infrared spectroscopy (GATR FT-IR). Spectroscopic measurements allow the assessment of wire orientation and structural integrity upon anchoring and casting into silica nanolayers, and to estimate the wire density. Moreover, the work provides a basis for monitoring the structural and orientation integrity of the membrane embedded wires upon

exposure to the sustained flux of electrons and protons during photocatalytic operation.

2. Experimental Section

Synthetic materials and methods. All chemicals were purchased from Sigma-Aldrich including HPLC grade (99.8%) solvents, which were dried with 3Å molecular sieve (Alfa-Aesar) for three days and stored in a nitrogen glovebox before use, unless noted otherwise. Hole conducting molecular wires of type oligo *p*-(phenylene vinylene) consisting of three units (abbreviated PV3) asymmetrically functionalized with one sulfonyl group on one end and one carboxy group on the opposite end, namely, Cesium 4-((E)-4-((E)-4-sulfonatostyryl)styryl)benzoate (Cs₂PV3_SO₃_CO₂), were synthesized according to the general methods described in previous work.⁵

Pt deposition. Two nm Ti adhesive layer and 100 nm of Pt (99.99%) were consecutively deposited by e-beam evaporation (Semicore SC600 e-beam evaporator) at $<2 \times 10^{-6}$ Torr on a Si wafer (prime grade p-type, Addison Engineering Inc.) pre-cleaned by standard RCA procedure.

Co₃O₄ deposition. Atomic layer deposition (ALD) of cobalt oxide was carried out using Oxford FlexAl-Plasma Enhanced Atomic Layer Deposition system situated in a Class 1000 cleanroom. The process temperature is 40°C, and

bis(cyclopentadienyl)cobalt(II) (cobaltocene, CoCp₂; min 98% STREM Chemicals Inc.) is used as precursor, heated to 80°C and bubbled with 200 sccm high purity Ar during pulse. Oxygen flow and chamber pressure were maintained at 60 sccm and 15 mTorr during the deposition process. CoCp₂ dose was 5 s long, followed by 5 s of purging. Oxygen plasma half-cycle was 1 s pre-plasma, 5 s plasma (300 W) and 15 sec purging. Fifty such cycles were deposited, which corresponds to 3.5 nm thickness of Co₃O₄. AFM images of 3.5 nm Co₃O₄ ALD layers reported in previous work exhibit a surface roughness RMS = 0.28 nm.⁴

Thickness measurement. The thickness of ALD oxide films were measured using spectroscopic ellipsometry (Horiba Jobin UVISSEL) in the 900-250 nm range at angles varying from 45 to 70° with 5° steps.

Anchoring of 4-(Trimethoxysilyl)aniline (TMSA) on Co₃O₄. 1.5 x 3 cm² Si/Pt/Co₃O₄ substrates were cleaned by sonication in isopropanol for 5 min before being placed in a flask containing 5.4 mg (0.025 mmol) TMSA and 50 mL toluene (90%, Gellest (10% 3-(trimethoxysilyl)aniline)). The solution was refluxed for 4 h. After cooling, the substrates were transferred directly to fresh tetrahydrofuran, sonicated for 10 min, and the solvent was switched to water and refluxed for 1 h. As a final step, the substrates were dried with a N₂ stream and immediately utilized for PV3 attachment or kept in a closed vial for further characterization.

Covalent attachment of PV3. Si/Pt/Co₃O₄ substrate with TMSA attached was placed in a desiccator. 1.0 mg (2.0 μmol) of PV3 and 0.8 mg (2.2 μmol) of HATU (O-(7-Azabenzotriazol-1-yl)-N,N,N',N'-tetramethyluronium-hexafluorophosphate) were sealed in a Schlenk flask and evacuated on the Schlenk line for 2 hours before 1 mL dimethyl formamide (anhydrous; Sigma Aldrich) was added by syringe. The solution was stirred for 30 minutes until it became bright yellow. The solution was dropped onto the substrate and the desiccator evacuated and refilled with nitrogen. The procedure was repeated 3 times. After 24 h the substrate was rinsed with water and transferred to a flask containing deionized water, sonicated for 5 min, and dried in N₂.

SiO₂ deposition. Silicon dioxide layers were deposited with a modified Savannah 100 Cambridge Nanotech ALD system equipped with a 300 W hollow cathode plasma source (Meaglow, Inc.) and a grounding grid above the sample. SiO₂ deposition was carried out at 40°C with 150 W plasma power using the following cycle: Under a flow of 5 sccm of Ar the chamber exhaust was closed and a 0.05 s pulse of tris(dimethylamino)silane (3DMSA) introduced to the chamber. The chamber was kept sealed for 60 s before purging with 40 sccm of Ar for 30 s followed by a 5 sccm 45 s purge with O₂. At a pressure of ~200 mTorr the plasma was ignited for 5 s followed by purging with Ar for 45 s at 5 sccm. Twenty such cycles lead to a deposition of 3.78 ± 0.04 nm thick SiO₂ layer. Cross sectional HR-TEM and AFM images of

silica nanolayers deposited by the plasma-enhanced ALD method on Pt reported in a preceding paper demonstrate uniformity,⁹ while a scanning TEM-EDX image of a SiO₂ ALD layer grown on Co₃O₄ nanolayer shows uniformity as well (Figure 3A of Ref. 4). Conformal property of the SiO₂ layers was shown by O₂ blocking and suppression of redox activity of standard redox couples such as ferrocene or ferrocyanide.^{4,9,10} An atomic Si/O ratio of 0.51 ± 0.05 for the silica ALD layer was determined by high resolution XPS of an SiO₂ layer deposited on bare Pt (Figure S4).

FT-IRRAS measurements: IRRAS spectra were recorded on a Bruker FT-IR spectrometer model Vertex 80 equipped with a LN₂ cooled HgCdTe detector Kolmar model KMPV11-1-J2 with a 14 μm band gap or KMPV8-1-J2 with 8 μm bandgap, a computer controlled reflection accessory Bruker model A513/QA, and wire-grid polarizer model F350. The mirror angle of the IRRAS accessory was fixed at 78° and the grid polarizer switched between p and s polarization, and an aperture of 2.5 mm was used. Twenty spectra of 400 scans each at 2 cm⁻¹ resolution were recorded and averaged. Sample single beam spectra with p polarization were divided by single beam spectra of reference sample (mirror) and the negative logarithm calculated. A corresponding absorbance spectrum for the s polarized configuration was computed and subtracted from the p polarized absorbance spectrum.

$$-^{10}\log(p, \text{ sample/p, ref}) - [-^{10}\log(s, \text{ sample/s, ref})]$$

From this result, a background was subtracted which is specified in the corresponding Figure caption for each spectrum shown in Sect. 3. The background absorbance spectrum was determined by the same computational method as used for the sample. All figures show spectra calculated according to this method, unless noted otherwise. Bands of residual atmospheric water vapor in the sample compartment were computationally eliminated as well. In some cases, baseline correction using a polynomial function was conducted to facilitate comparison of spectra. This information is described in Figure captions where applicable.

Grazing angle ATR FT-IR measurements. Spectra were recorded on the same Vertex 80 instrument described above equipped with a Harrick VariGATR grazing angle accessory with Ge single reflection ATR crystal and force sensor for accurate and reproducible compression of the sample against the ATR crystal. All spectra were recorded at 61° incident angle and 2 cm^{-1} resolution. ATR crystal/air spectra were used as reference.

The geometry of GATR FT-IR and FT-IRRAS measurement configurations for a Si/Pt/Co₃O₄ sample with PV3 embedded in SiO₂ is shown in Figure 1.

3. Results and Discussion

Comparison of polarized with non-polarized FT-IR spectra of Co_3O_4 surfaces with tripodal anchors before and after attachment of wire molecules, and upon casting into ultrathin silica layers will be presented and discussed in turn.

3.1 Structure and Orientation of Anchor on Co Oxide Surface.

Spectra of the TMSA anchored on a flat Co_3O_4 surface prepared by ALD on Pt recorded by FT-IRRAS and GATR FT-IR spectroscopy are shown in Figure 2 trace (a) and (b), respectively. Mode assignment is aided by the FT-IR transmission spectrum of TMSA crystallites pressed into a KBr wafer presented in Figure 3. In the fingerprint region, the NH_2 bending mode at 1626 cm^{-1} and quadrant and semicircle stretching modes of the aromatic ring at 1604 , 1512 and 1420 cm^{-1} observed for solid TMSA⁵ exhibit only minor shifts upon anchoring on the Co oxide surface, with corresponding absorptions at 1621 , 1602 , 1510 , 1420 cm^{-1} as shown in Figure 2(a) (background spectra employed are presented in Figure S1; modes at 1431 and 1488 cm^{-1} are due to small amounts of the meta isomer of TMSA)⁵. The absorption at 1272 cm^{-1} , with shoulder at 1293 cm^{-1} , is typical for the phenyl C-N stretch mode.¹¹ The region below 1200 cm^{-1} features new bands originating from surface attachment. While the 1193 cm^{-1} peak is observed both for crystal and surface anchored TMSA and assigned to in-plane phenyl C-H bending mode,¹¹ the intense broad absorption with a maximum at 1139 cm^{-1} and shoulders at 1107 and 1050 cm^{-1} are unique to the Co oxide anchored species. Because

this is the typical region for Si-O stretch absorptions, the features are assigned to the stretching Si-O-Co modes of the tripodal Si(-O-Co)₃ anchor. The intense bands obscure much weaker phenyl C-H bending modes, some with admixed phenyl C-Si stretch, between 1150 and 1000 cm⁻¹.^{11,12} The $\nu(\text{Si}(-\text{O}-\text{Co})_3)$ bands replace the Si-O-C modes of the silyl trimethoxy moiety of free TMSA at 1129 (admixed phenyl C-Si stretch) and 1067 cm⁻¹ shown in Figure 3.

The region above 2000 cm⁻¹ shows the weak TMSA aryl CH stretch at 3030 cm⁻¹ along with asymmetric and symmetric NH₂ stretch modes with maxima at 3364 and 3221 cm⁻¹, respectively, in its expected positions (Figure S2(a)).^{12,13} Most noteworthy is the absence of CH stretch modes associated with TMSA molecules featuring residual methoxy groups, as displayed in Figure S2 trace (a). Specifically, methoxy group absorptions at 2940 and 2839 cm⁻¹ shown in the spectrum of pure TMSA sample prior to anchoring (Figure S2 trace (b)) are not observed, consistent with the absence of merely partially (mono or dipodally) anchored TMSA molecules.

Comparison of the IRRAS spectra with GATR FT-IR measurements of the same sample of TMSA anchored on a planar Co₃O₄ film shown in Figure 2 trace (b), for which infrared probe light is not polarized (the evanescent wave is absorbed by vibrational modes with transition moments perpendicular and parallel to the Pt surface), provide insight into the orientation of the anchored molecules. In the IRRAS measurement, the metal surface selection rule allows probe light absorption exclusively for the component of a

vibrational mode perpendicular to the surface, while no light is absorbed by horizontal vibrational components parallel to the surface.^{14,15} Therefore, recording of IRRAS with p-polarized light shows the perpendicular component of infrared modes while s-polarized light does not show any bands of surface anchored molecules. As can be seen from Figure 2(b), in-plane modes (with respect to the aryl ring) at 1621, 1602, 1510, 1420, 1288 cm^{-1} , 1263 cm^{-1} and 1193 cm^{-1} in the GATR FT-IR spectrum exhibit similar relative intensity as in the p-polarized IRRAS spectrum, as would be expected for orientation of the molecular axis perpendicular to the Co oxide plane (Figure 4). An exception appears to be the intensity distribution between the two components assigned to the C-N stretch at 1263 cm^{-1} and 1288 cm^{-1} which is different in the two spectra, but this is due to a background feature of the Pt reflection mirror (Figure S1c) that results in additional intensity for the 1263 cm^{-1} band in the case of the GATR FT-IR spectrum. The SiOCo stretch modes on the 1140 – 1000 cm^{-1} region give rise to the most intense absorption in polarized and non-polarized spectra. However, the integrated intensity of the $\nu(\text{SiOCo})$ absorption in the GATR FT-IR spectrum relative to the PV3 in-plane modes above 1200 cm^{-1} is substantially larger than in the IRRAS trace, and the absorption profiles between 1140-1000 cm^{-1} look different in the two spectra. This is to be expected for tripodal anchoring with the aryl plane perpendicular to the oxide surface because the dipole moment changes associated with SiOCo stretch vibrations possess both p and s components, resulting in more absorption of non-polarized infrared light by these modes.

Furthermore, the contribution of $\nu(\text{SiOCo})$ modes to each individual normal mode in the 1140-1000 cm^{-1} region determines the p- versus s-distribution, which is the origin of different relative intensities for the p-polarized and non-polarized spectra.

The most distinct difference between spectra with polarized and non-polarized infrared light is the intense out-of-plane aryl C-H mode at 885 cm^{-1} ^{11,13} in the GATR FT-IR spectrum that is absent in the IRRAS. This mode is not expected to be observed by p-polarized light if the molecular axis of anchored TMSA is in perpendicular orientation because the dipole moment change is parallel to the Pt surface. Based on the observed intensity behavior of aryl in- and out-of-plane infrared modes and tripodal anchor vibrations under polarized and non-polarized probe light, we conclude that TMSA anchor molecules have upright orientation on the Co oxide surface.

The GATR FT-IR spectrum allows for an estimate of the surface density of anchored TMSA molecules. Using the measured peak absorbance $A = 0.00058$ for the aryl stretch mode at 1602 cm^{-1} (Figure 2(b)) and the extinction coefficient of $\epsilon = 347 \text{ L mol}^{-1} \text{ cm}^{-1}$ obtained by IR spectroscopy of TMSA in solution, the Beer-Lambert law¹⁶ gives surface coverage $A/\epsilon = 1.7 \times 10^{-9} \text{ mol cm}^{-2}$ or 10 molecules nm^{-2} geometrical area. Because the uniform ALD layer consists of Co_3O_4 particles of 3-5 nm diameter with freely accessible surface between particle boundaries,⁴ this corresponds to 2 to 3 TMSA nm^{-2} actual surface.

3.2 Orientation of Attached PV3 Wire. Attachment of PV3 wire molecules to Co_3O_4 -anchored TMSA via amide linkage results in the IRRAS spectra presented in Figure 5 trace (b). For comparison, the spectrum of TMSA before wire attachment is shown in the same Figure (trace (a), replicated from Figure 2(a)). Successful attachment of the wire molecules is manifested by the nearly complete disappearance of the free NH_2 mode of TMSA at 1621 cm^{-1} under concurrent growth of an amide I band at 1666 cm^{-1} . The observed residual 1621 cm^{-1} absorption of free TMSA is attributed to anchor molecules that are not accessible for amide linkage formation to PV3 (typically about 10 percent of anchored TMSA).

Spectral changes upon PV3 attachment are most clearly visualized by subtracting the spectrum of anchored TMSA before linkage to PV3 from the spectrum after attachment, shown as trace (c) of Figure 5. All modes of the TMSA anchor, observed before PV3 attachment at 1621 , 1510 , 1488 , 1431 , 1420 , 1293 , 1272 , and 1193 cm^{-1} , appear as negative bands, with the decreasing 1293 and 1272 cm^{-1} $\nu(\text{CN})$ peaks slightly red-shifted because of overlap with increasing $\nu(\text{CN})$ bands after formation of the amide bond. The absence of any intensity change of the SiOCo stretch modes at 1139 , 1107 and 1050 cm^{-1} confirms that the structure of the tripodal anchor remains unchanged upon wire attachment. At the same time, absorption peaks of attached PV3 wire grow in at 1666 (amide I), >1581 ($\nu(\text{CC})$ aryl), 1521 (amide II), 1392 ($\nu(\text{CC})$ aryl), 1321 ($\nu_{\text{as}}(\text{SO}_3\text{H})$), 1284 ($\nu(\text{C-N})$), 1261 ($\nu(\text{C-N})$), 1122 ($\nu(\text{C-S})$, $\nu_{\text{sym}}(\text{SO}_3^-)$),¹³ 1033 cm^{-1} (in plane alkenyl $\delta(\text{C=C-H})$), $\nu(\text{CC})$,

$\nu_{\text{sym}}(\text{SO}_3^-)$, and 1009 cm^{-1} (in plane alkenyl $\delta(\text{C}=\text{C}-\text{H})$, $\nu(\text{CC})$, $\nu(\text{C}-\text{S})$, $\nu_{\text{sym}}(\text{SO}_3^-)$).^{12,13,17}

Information about the detailed structure and orientation of the PV3 axis is gained by comparing p-polarized IRRAS spectra of the attached wire shown in Figure 6(c) (replicated from Figure 5(c)) with IRRAS of free, non-attached PV3 molecule physisorbed on the Co_3O_4 surface (Figure 6(b)), with non-polarized FT-IR transmission spectrum of the solid PV3 powder (Figure 6(a)), and with non-polarized GATR FT-IR of the attached PV3 (Figure 6(d)). Some differences among the spectra are due to the fact that the free wire molecule has a terminal CO_2^- substituent, which for the surface attached molecule is replaced by an amide group linked to a TMSA anchor. Specifically, the spectra of physisorbed PV3 (Figure 6(b)) and solid PV3 (Figure 6(a)) exhibit the intense asymmetric stretch of the carboxy group at 1544 cm^{-1} and a moderately strong symmetric CO_2^- stretch at 1419 cm^{-1} , both absent in the spectrum of the anchored wire, Figure 6(c). Another structural difference is a change of protonation state of the sulfonate substituent on the PV3 molecule. In the FT-IR of the solid sample (Figure 6(a)), the group is in the deprotonated SO_3^- state exhibiting a pair of bands at 1188 and 1221 cm^{-1} .^{13,17} By contrast, physisorbed (Figure 6(b)) and anchored PV3 (Figure 6(c)) on Co_3O_4 do not show these bands, but absorptions at 1321 cm^{-1} and 1307 cm^{-1} instead, respectively, characteristic for the asymmetric S-O stretch of the protonated SO_3H group.^{13,18} We attribute the protonation of the sulfonate group to the availability of protons from the Co_3O_4 surface, which is

consistent with the fact that Co-OH groups of Co oxide surfaces are distinctly acidic as indicated by a 100 cm^{-1} red shift of the OH stretch mode relative to alcohol OH groups, or 200 cm^{-1} compared to surface Si-OH groups.^{19,20}

Aside from these structural differences, the in-plane phenylene vinylene stretch and bending modes of physisorbed PV3 (Figure 6(b)) at 1594, 1125, 1102, 1040, 1009 exhibit only minor frequency shifts relative to corresponding absorptions of free PV3 (1590, 1125, 1100 (shoulder), 1035, and 1008 cm^{-1}) and covalently anchored PV3 (>1581 , 1122, 1033, 1009 cm^{-1}) indicating that the structure of the phenylene vinylene backbone is the same irrespective of surface adsorption or covalent attachment. By contrast, there is a marked difference regarding relative intensity within this subset of PV3 infrared bands when comparing the IRRAS of the anchored molecules (Figure 6(c)) with GATR FT-IR of the same sample (trace (d)), IRRAS of physisorbed PV3 (trace (b)), and PV3 powder FT-IR (trace (a)). Namely, the three modes at 1122, 1033 and 1009 cm^{-1} that feature contributions from $\nu_{\text{sym}}(\text{SO}_3^-)$, which has a significant component parallel to the oxide surface, have substantially lower intensity relative to the modes above 1200 cm^{-1} in the IRRAS of anchored wire especially in comparison with the non-polarized GATR FT-IR of the same sample and the IRRAS of physisorbed PV3. As the only modes with a significant out-of-(molecular) plane component, these are expected to exhibit reduced intensity under p-polarized probe light if the wire plane is perpendicular to the Co_3O_4 (and Pt) surface, as observed. Most noteworthy is the absence of a strong out-of-plane vinyl C=C-H bending mode known to

absorb in the 1000-900 cm^{-1} region^{12,21,22} in the IRRAS of anchored PV3, while the GATR FT-IR spectrum of the anchored PV3 sample,⁴ the IRRAS of physisorbed PV3 (Figure 6(b)), and the transmission spectrum of free wire Figure 6(a) all exhibit this mode prominently at 963 cm^{-1} . Because the out-of-plane mode is oscillating perpendicular to the aryl-vinyl plane of PV3, the absence under p-polarized infrared probe light but appearance for physisorbed PV3 where the molecular plane is parallel to the surface, strongly indicates that the wire axis of the anchored wire is oriented upright relative to the Co oxide (and Pt) surface. We conclude that the intensities of the infrared modes of the wire molecules under p-polarized probe light indicate perpendicular orientation of the molecules anchored on the Co_3O_4 surface.

A rough estimate of how close the wire molecules are to perpendicular orientation relative the Co_3O_4 (and Pt) plane can be made based the expression $\cos^2(\theta) = I_{\text{obs}}/3 I_{\text{iso}}$, where θ is the average angle between the wire infrared transition moment of a given mode and the surface normal, I_{obs} the observed intensity of the band in the IRRAS, and I_{iso} the observed intensity in the isotropic phase.²³ In our case, I_{obs} is taken as the spectral noise (peak-to-peak noise) of the IRRAS in the 960 cm^{-1} region, which is the frequency of the CH out-of-plane bending mode. Because the band is not observed, it constitutes an upper limit for I_{obs} . I_{iso} is approximated by the intensity of this band observed in the GATR FT-IR spectrum at 963 cm^{-1} because it is measured with non-polarized light in the absence of the surface dipole effect

and constitutes a lower limit for I_{iso} . With 0.000046 absorbance units for the peak-to-peak noise and GATR FT-IR intensity at 963 cm^{-1} of 0.00036, θ is calculated as 78 degree. Hence, the transition moment of the out-of-plane CH bending mode is 78 degree (or larger) relative to the surface normal, which implies that the average orientation of the wire molecule axis is tilted away from normal orientation to the surface by at most 12 degree.

It is important to note that the anchored wire molecules exhibited high thermal stability, as shown by IRRAS measurements upon heating of the Co_3O_4 layer with anchored PV3 molecules to 200 C for several hours. No loss of wire molecules occurred, with the only observed change being a small increase of the intense SiOCo stretch modes of the anchor in the $1140\text{-}1000\text{ cm}^{-1}$ region, most likely due to structural change of the Co_3O_4 surface upon heating.

3.3 Structural Integrity and Orientation of PV3 Wires upon Embedding into Silica.

The sensitive FT-IRRAS method allowed us to investigate the structural integrity and orientation of PV3 upon embedding into silica, and to optimize the ALD protocol for minimum interference of the deposition process with the organic. Silica ALD requires oxygen plasma for removal of residual organic ligands of 3DMAS precursor in place of the standard method of heating at temperatures in excess of 550 C ,²⁴ which is not be suitable in the presence of organic wires. Therefore, plasma exposure per ALD cycle needed to be

optimized to ensure complete ligand removal while minimizing damage to the anchored wire molecules. The optimized protocol is presented in Sect. 2, and infrared evidence for the complete removal of residual organic Si precursor ligands shown in Figure 2(a) of a previous publication.⁸ Figure 7(a) compares IRRAS spectra of PV3 anchored on Co₃O₄ before silica casting (black trace (1)), after 20 cycles silica ALD (red trace (2)), and a total of 40 silica ALD cycles (blue trace (3)) (for clarity, different absorbance scales are used for bands above and below 1200 cm⁻¹). Inspection of the intensity of all PV3 absorptions before and after the first 20 cycles of silica deposition indicates an absorbance loss of 20 ± 3 percent. While no infrared bands of organic decomposition products were detected, the loss of PV3 intensity is most likely due to attack of active oxygen species produced by the plasma pulse. The absence of infrared bands of breakdown products is attributed to removal by the Ar purge pulse that follows the O₂ plasma pulse. Comparison of the PV3 bands after silica ALD of additional 20 cycles (Figure 7(a), trace (3)) shows no further absorbance loss, consistent with the conclusion that the wire molecules are completely embedded in silica already after the initial 20 ALD cycles. This is in agreement with the silica layer thickness for 20 cycles of 3.78 ± 0.04 nm determined by ellipsometry.

A pronounced new infrared band upon casting of silica is the longitudinal optical (LO) SiOSi stretch mode of the silica nanolayer at 1235 cm⁻¹²⁴⁻²⁷ (Figure 7(a) traces (2) and (3)) as described in detail in a previous report⁸ and reproduced for convenience as Figure S3 in this paper. The

transverse (TO) SiOSi mode gives rise to shoulders in the 1150-1050 cm^{-1} region,⁸ but is strongly overlapped here by SiOCo stretch modes of the Si(-O-Co)₃ anchor moiety of the wire with maximum at 1139 cm^{-1} and shoulders at 1107 and 1050 cm^{-1} (Figure 7(a), trace (1)). Comparison of the intensity of the 1235 cm^{-1} silica band for 20 cycle and 40 cycle layers shows that the silica absorbance grows linearly with numbers of ALD cycles, providing a convenient measure of the relative amounts of silica deposited. It is important to note that no organic residues of the ALD precursor 3DMAS with its known characteristic CH absorption in the 2800 - 3000 cm^{-1} region are found,²⁴ which confirms that the ALD protocol optimized for maintaining molecular wire integrity fulfils simultaneously the requirements for complete removal of precursor ligands.

Changes of PV3 infrared bands upon silica casting are directly visualized by comparing the IRRAS spectrum of the attached wire molecules before silica casting, shown in Figure 7(a) trace (1), with the spectrum after deposition of SiO₂ from which the bands due to 20 ALD cycles of SiO₂ are removed by computational subtraction. The IRRAS of 20 cycles of SiO₂ was obtained by calculating the difference of the 40 cycle silica spectrum (trace (3) of Figure 7(a)) and the 20 cycle silica layer (trace (2) of Figure 7(a)). The result is shown in Figure 7(b) trace (2) along with the spectrum of the same sample before silica casting (trace (1)). The relative intensity of the (p-polarized) PV3 modes before and after deposition of 20 ALD SiO₂ cycles remains unchanged within uncertainty, indicating that the orientation of the

axis of the wire molecules does not change significantly upon silica casting. Specifically, amide I, amide II absorption and aryl CC stretch absorption bands in the 1700 – 1300 cm^{-1} region are completely unchanged upon silica casting. The broad SO_3H stretch at 1325 cm^{-1} is slightly more intense in the SiO_2 environment possibly because of hydrogen bonding interaction with the silica environment. A marked change upon silica deposition is the stronger absorption in the 1130-1050 cm^{-1} range, which before deposition is dominated by the $\text{Si}(\text{OCo})_3$ stretch modes of the TMSA anchor. Upon silica ALD, SiOCo bonds at the new $\text{Co}_3\text{O}_4\text{-SiO}_2$ interface are formed⁸ that give rise to the additional absorption in SiOCo stretch region. The only spectral region that shows additional changes is between 1200 and 1250 cm^{-1} where the intense SiOSi LO mode of silica absorbs; any attribution to spectral changes of PV3 is difficult to discern because of the uncertainty of spectral subtraction of the intense LO band. From these IRRAS observations, we conclude that, upon casting into ultrathin SiO_2 layer, the structure and orientation of PV3 wire molecules are preserved with high fidelity.

4. Conclusions

Comparison of infrared spectra of molecular wires anchored on Co oxide catalyst surface and embedded in ultrathin silica membranes using polarized and non-polarized probe light with two surface sensitive techniques, IRRAS FT-IR and grazing angle ATR FT-IR, provide the first experimental

observations on their spatial orientation. Distinct intensity differences of group modes observed with the two methods of infrared probing revealed preferred perpendicular orientation of the anchored wire molecules relative to the Co oxide surface. In addition to the use of tripodal $\text{Si}(\text{OCo})_3$ anchors, the upright orientation may be enforced by the ALD process itself because SiO_2 grows on the metal oxide surface in the free spaces between the anchored organic molecules²⁸ with tendency to straighten them up. The high sensitivity of the IRRAS method allowed us to explore and identify ALD synthesis conditions that result in minimal damage to the organic wire molecules during silica casting. These complementary surface sensitive infrared methods constitute a powerful approach for elucidating the structure and orientation of surface anchored molecules.

IRRAS measurements demonstrate the preservation of the structure and orientation of the anchored wire molecules with high fidelity upon casting into ultrathin silica layers. By using the Pt mirror as working electrode in an FT-IRRAS spectroelectrochemical cell, the spectroscopic technique will enable in situ monitoring of the structural and orientation integrity of the silica embedded molecular wires under the sustained electron and proton flux conditions of photocatalytic operation.

Supporting Information

Single polarization FT-IRRAS of all samples; FT-IRRAS and GATR FT-IR spectra of solid material components used for background subtraction; FT-IR spectra of molecular precursors.

Acknowledgment

Funding to support this work was provided by the Energy & Biosciences Institute through the EBI-Shell program. Portions of this work (plasma enhanced atomic layer deposition, ellipsometry, e-beam evaporation) were performed as a User Project at The Molecular Foundry, Lawrence Berkeley National Laboratory, which is supported by the Office of Science, Office of Basic Energy Sciences, of the U.S. Department of Energy under Contract No. DE-AC02-05CH11231. We thank Dr. Eran Edri for XPS measurement of the ALD silica layers.

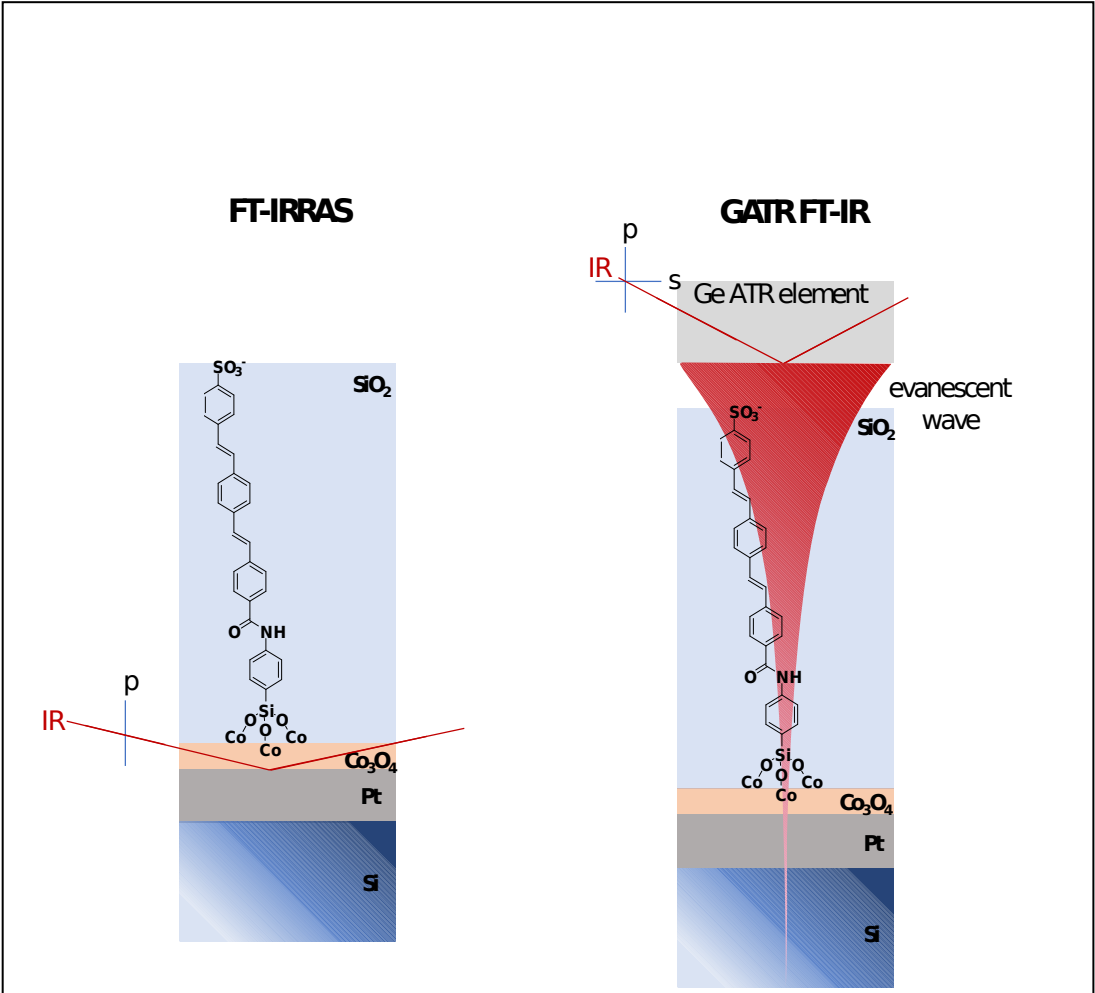
References

- [1] Edri, E.; Aloni, S.; Frei, H. Fabrication of Core-Shell Nanotube Array for Artificial Photosynthesis Featuring an Ultrathin Composite Separation Membrane. *ACS Nano* **2018**, *12*, 533-541.
- [2] Soo, H. S.; Agiral, A.; Bachmeier, A.; Frei, H. Visible Light-Induced Hole Injection into Rectifying Molecular Wires Anchored on Co_3O_4 and SiO_2 Nanoparticles. *J. Am. Chem. Soc.* **2012**, *134*, 17104-17116.
- [3] Agiral, A.; Soo, H. S.; Frei, H. Visible Light-Induced Hole Transport from Sensitizer to Co_3O_4 Water Oxidation Catalyst across Nanoscale Silica Barrier with Embedded Molecular Wires. *Chem. Mater.* **2013**, *25*, 2264-2273.
- [4] Edri, E.; Frei, H. Charge Transport Through Organic Molecular Wires Embedded in Ultrathin Insulating Inorganic Layer. *J. Phys. Chem. C* **2015**, *119*, 28326-28334.
- [5] Katsoukis, G.; Frei, H. Heterobinuclear Light Absorber Coupled to Molecular Wire for Charge Transport across Ultrathin Silica Membrane for Artificial Photosynthesis. *ACS Appl. Mater. Interfaces* **2018**, *10*, 31422-31432.
- [6] Katsoukis, G.; Frei, H. Ultrathin Oxide Layers for Nanoscale Integration of Molecular Light Absorbers, Catalysts, and Complete Artificial Photosystems. *J. Chem. Phys.* **2019**, *150*, 041501.
- [7] Edri, E.; Cooper, J. K.; Sharp, I. D.; Guldi, D. M.; Frei, H. Ultrafast Charge Transfer between Light Absorber and Co_3O_4 Water Oxidation Catalyst

- across Molecular Wires Embedded in Silica Membrane. *J. Am. Chem. Soc.* **2017**, *139*, 5458-5466.
- [8] Jo, W. J.; Katsoukis, G.; Frei, H. Proton Conductivity and O₂ Impermeability of Ultrathin Oxide Multilayers with Built-in Silica Separation Membrane for Nanoscale Artificial Photosystems. *J. Am. Chem. Soc.*, submitted.
- [9] Yuan, G.; Agiral, A.; Pellet, N.; Kim, W.; Frei, H. Inorganic Core-Shell Assemblies for Closing the Artificial Photosynthetic Cycle. *Faraday Discuss.* **2014**, *176*, 233-249.
- [10] Cornejo, J. A.; Sheng, H.; Edri, E.; Ajo-Franklin, C. A.; Frei, H. Nanoscale Membranes that Chemically Isolate and Electronically Wire Up the Abiotic/Biotic Interface. *Nature Commun.* **2018**, *9*:2263.
- [11] Evans, J. C. The Infrared Spectrum of Aniline. *Spectrochim. Acta* **1960**, *16*, 438.
- [12] Bellamy, L. J. *The Infrared Spectra of Complex Molecules*; Chapman and Hall: London, 1975; Vol. 1.
- [13] Colthup, N. B.; Daly, L. H.; Wiberley, S. E. *Introduction to Infrared and Raman Spectroscopy*; Academic Press: London, 1990.
- [14] Hollins, P. In *Encyclopedia of Analytical Chemistry*; R. A. Meyers, Ed.; Wiley: New York, 2006; p 1.
- [15] Chabal, Y. J. Surface Infrared Spectroscopy. *Surf. Sci. Rep.* **1988**, *8*, 211-357.

- [16] Bramblett, A. L.; Boeckl, M. S.; Hauch, K. D.; Ratner, B. D.; Sasaki, T.; Rogers, J. W. Determination of Surface Coverage for Tetraphenylporphyrin Monolayers Using Ultraviolet Visible Absorption and X-ray Photoelectron Spectroscopies. *Surf. Interface Anal.* **2002**, *33*, 506-515.
- [17] Shishlov, N. M.; Khursan, S. L. Effect of Ion Interactions on the IR Spectrum of Benzenesulfonate Ion. Restoration of Sulfonate Ion Symmetry in Sodium Benzenesulfonate Dimer. *J. Mol. Struct.* **2016**, *1123*, 360-366.
- [18] Socrates, G. *Infrared and Raman Characteristic Group Frequencies*; Wiley: New York, 2001; p 221.
- [19] Han, H.; Frei, H. Visible Light Absorption of Binuclear TiOCo^{II} Charge-Transfer Unit Assembled in Mesoporous Silica. *Microporous Mesoporous Mater.* **2007**, *103*, 265-272.
- [20] Bellamy, L. J. *The Infrared Spectra of Complex Molecules*; Chapman and Hall: London, 1980; Vol. 2, p 92.
- [21] Tian, B.; Zerbi, G.; Schenk, R.; Muellen, K. Optical Spectra and Structure of Oligomeric Models of Polyparaphenylenevinylene. *J. Chem. Phys.* **1991**, *95*, 3191-3197.
- [22] Hrenar, T.; Mitric, R.; Meic, Z.; Meier, H.; Stalmach, U. Vibrational Spectra and DFT Calculations of PPV-Oligomers. *J. Mol. Structure* **2003**, *661*, 33-40.

- [23] Allara, D. L.; Nuzzo, R. G. Spontaneously Organized Molecular Assemblies. Quantitative Infrared Spectroscopic Determination of Equilibrium Structures of Solution-Adsorbed n-Alkanoic Acids on an Oxidized Aluminum Surface. *Langmuir* **1985**, *1*, 52-66.
- [24] Burton, B. B.; Kang, S. W.; Rhee, S. W.; George, S. M. SiO₂ Atomic Layer Deposition Using Tris(dimethylamino)silane and Hydrogen Peroxide Studied by In Situ Transmission FT-IR Spectroscopy. *J. Phys. Chem. C* **2009**, *113*, 8249-8257.
- [25] Almeida, R. M.; Pantano, C. G. Structural Investigation of Silica Gel Films by Infrared Spectroscopy. *J. Appl. Phys.* **1990**, *68*, 4225-4232.
- [26] Pena, L. F.; Nanayakkara, C. E.; Mallikarjunan, A.; Chandra, H.; Xiao, M.; Lei, X.; Pearlstein, R. M.; Derecskei-Kovacs, A.; Chabal, Y. J. Atomic Layer Deposition of Silicon Dioxide Using Aminosilanes Di-sec-butylaminosilane and Bis(tert-butylamino)silane with Ozone. *J. Phys. Chem. C* **2016**, *120*, 10927-10935.
- [27] Tian, R.; Seitz, O.; Li, M.; Hu, W.; Chabal, Y. J. Infrared Characterization of Interfacial Si-O Bond Formation on Silanized Flat SiO₂/Si Surfaces. *Langmuir* **2010**, *26*, 4563-4566.
- [28] Son, H. J.; Wang, X.; Prasittichai, C.; Jeong, N. C.; Aaltonen, T.; Gordon, R. G.; Hupp, J. T. Glass-Encapsulated Light Harvesters: More Efficient Dye-Sensitized Solar Cells by Deposition of Self-Aligned, Conformal, and Self-Limited Layers. *J. Am. Chem. Soc.* **2012**, *134*, 9537-9540.



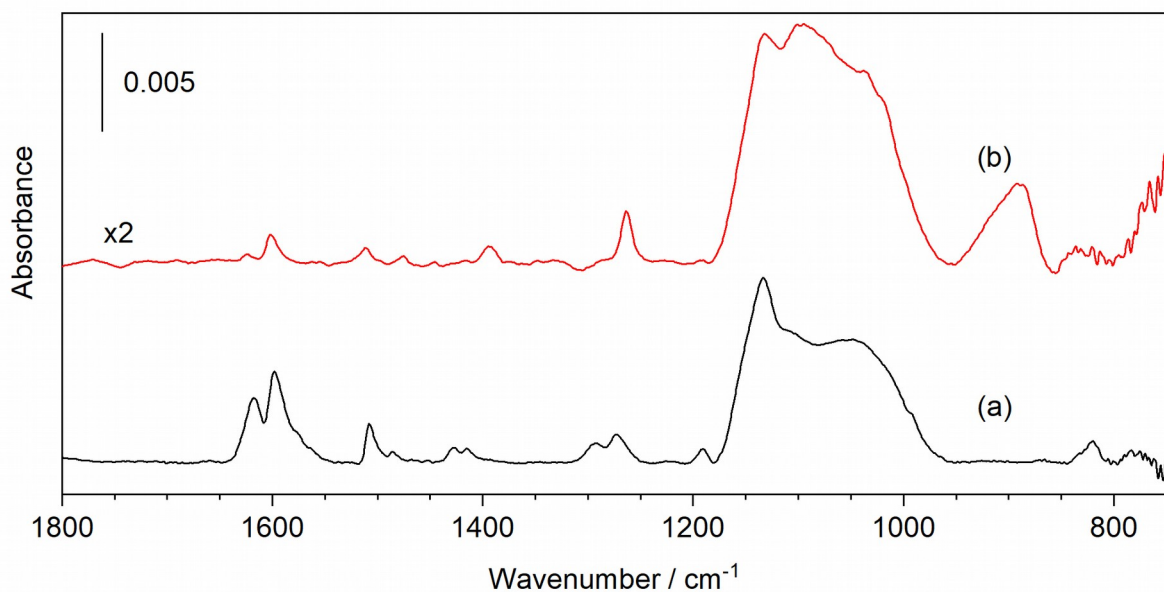


Figure 2: Polarized and non-polarized FT-IR spectra of TMSA anchored on Pt-Co₃O₄. (a) IRRAS for which Pt-Co₃O₄ background was subtracted. Baseline correction was applied using polynomial function. (b) GATR FT-IR of same sample.

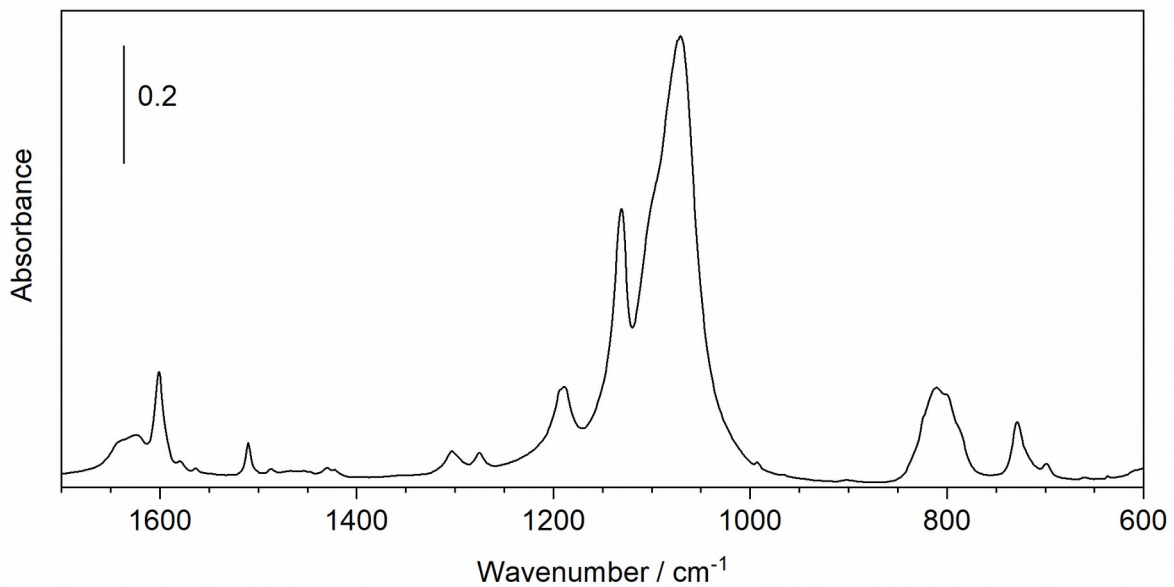
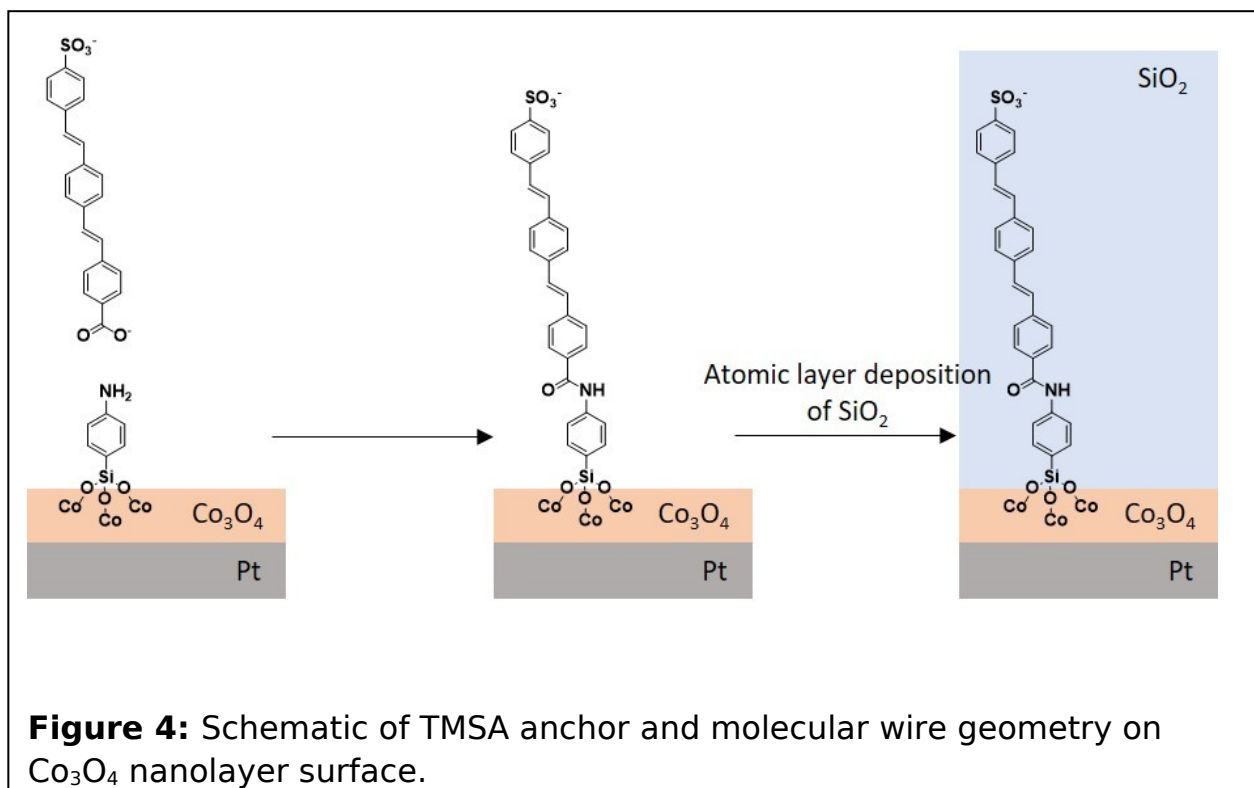


Figure 3: FT-IR absorbance spectrum of pressed KBr wafer of TMSA solid powder measured in transmission mode.



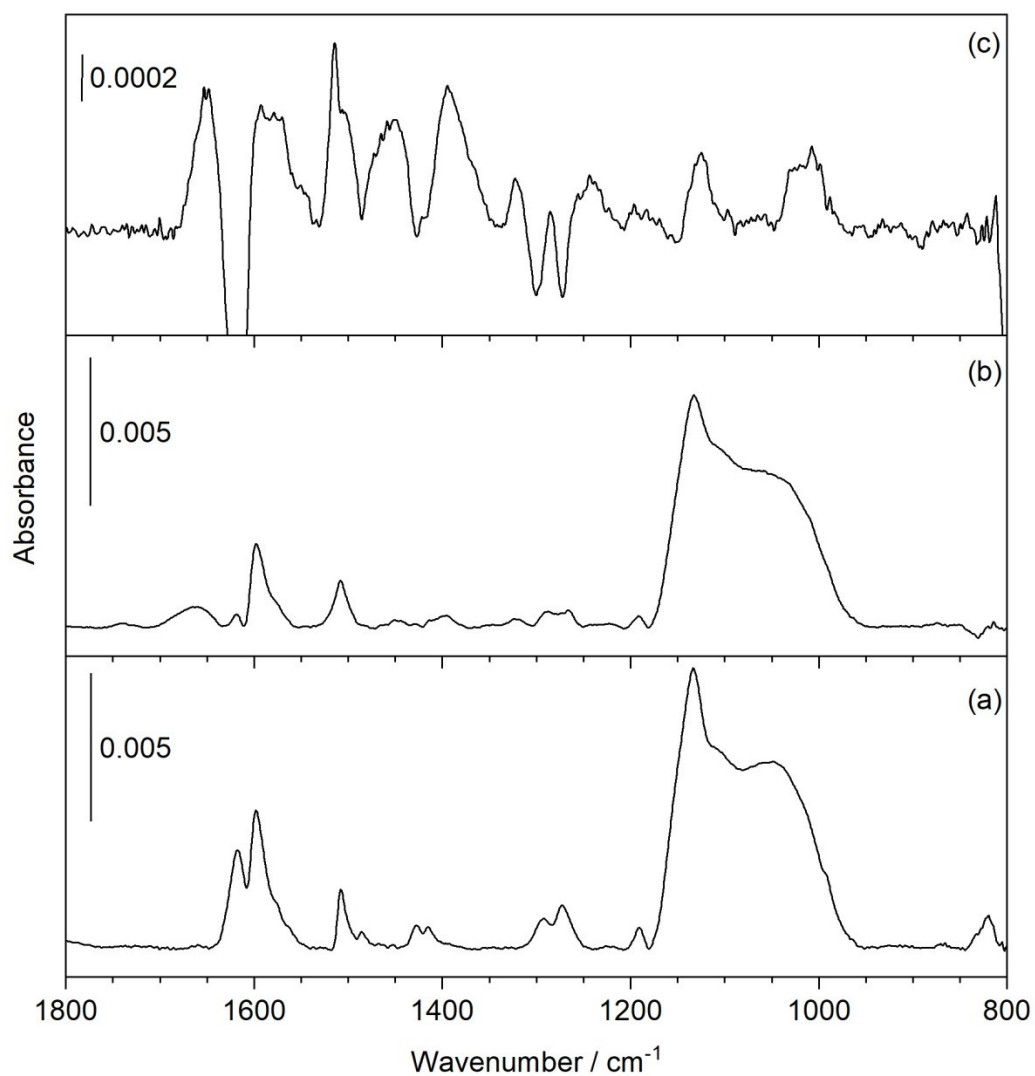


Figure 5: IRRAS of PV3 molecular wire attached to TMSA anchor on Co_3O_4 surface. (a) TMSA anchored on $\text{Pt-Co}_3\text{O}_4$ (replicated from Figure 1(a) for convenience). (b) After attachment of PV3. (c) Spectrum of attached PV3 (b) after subtraction of TMSA spectrum (a) and baseline correction with a polynomial. The weak absorption at 1736 cm^{-1} is not reproducible, it does not belong to the spectrum of anchored wire molecules.

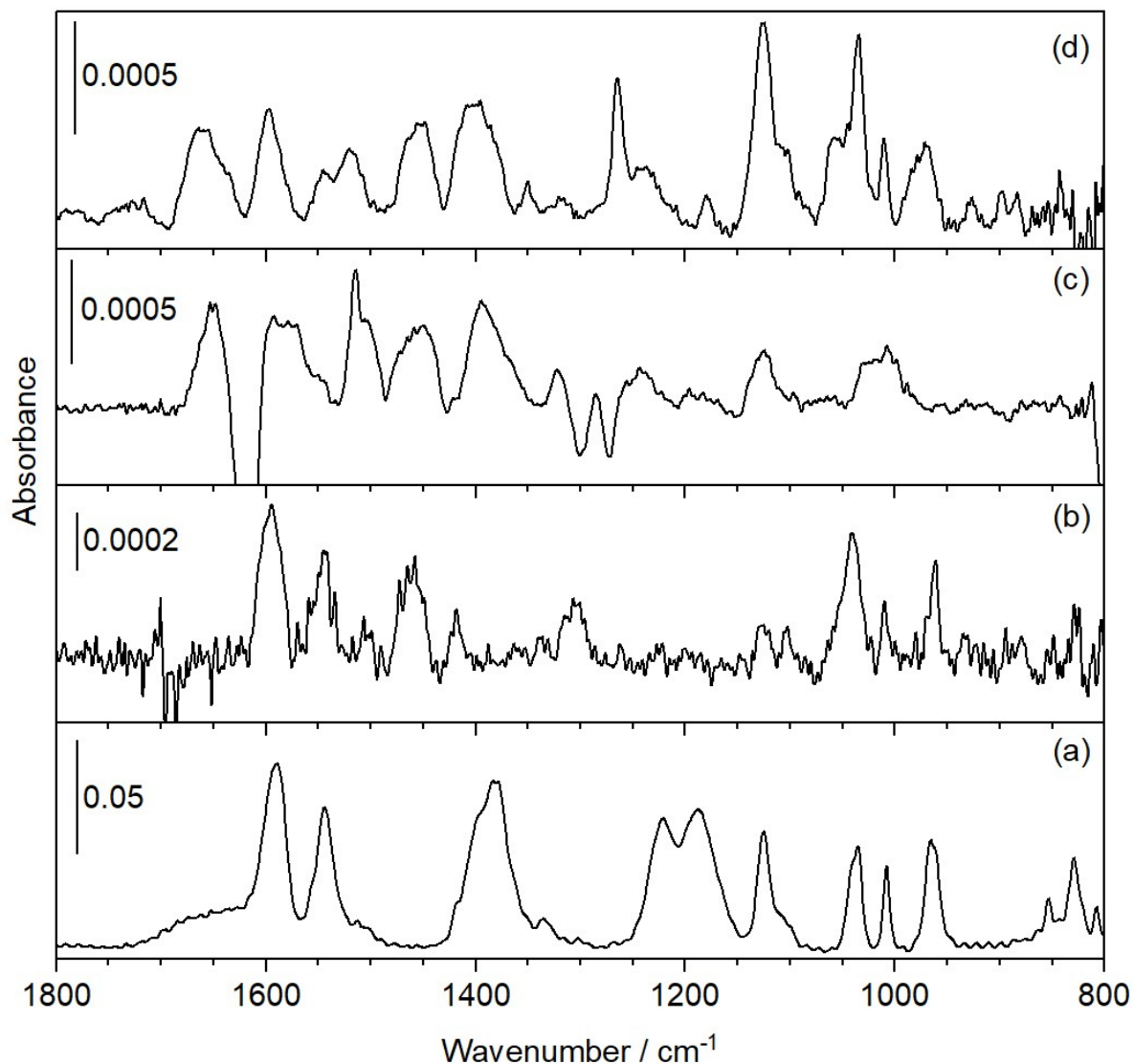


Figure 6: Comparison of FT-IR spectra of PV3 wire molecules. (a) FT-IR transmission spectrum of PV3 powder in KBr. (b) IRRAS of PV3 molecules physisorbed onto Pt-Co₃O₄ surface. (c) IRRAS of attached PV3 (Figure 5b) after subtraction of TMSA spectrum (Figure 5a) and baseline correction with a polynomial (replicated from Figure 5(c) for convenience). (d) GATR FT-IR of same sample as used in (c). Pt-Co₃O₄(3.5 nm)-TMSA was subtracted and baseline correction with a polynomial applied. The GATR FT-IR spectrum of the Pt-Co₃O₄ background is shown in Figure

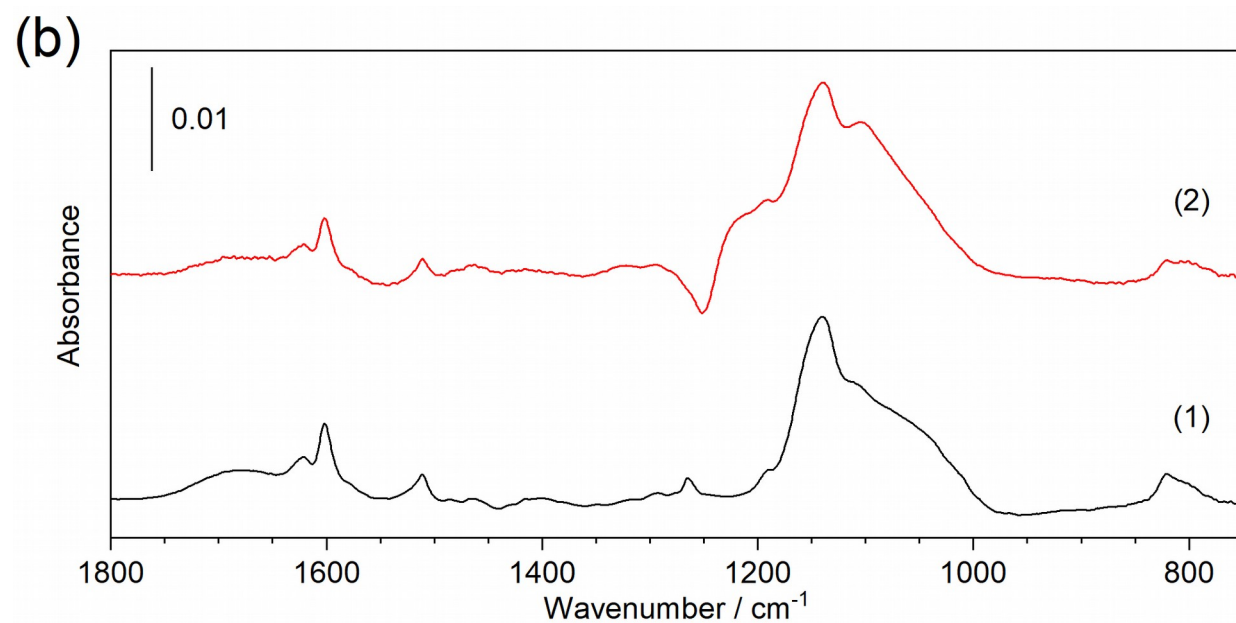
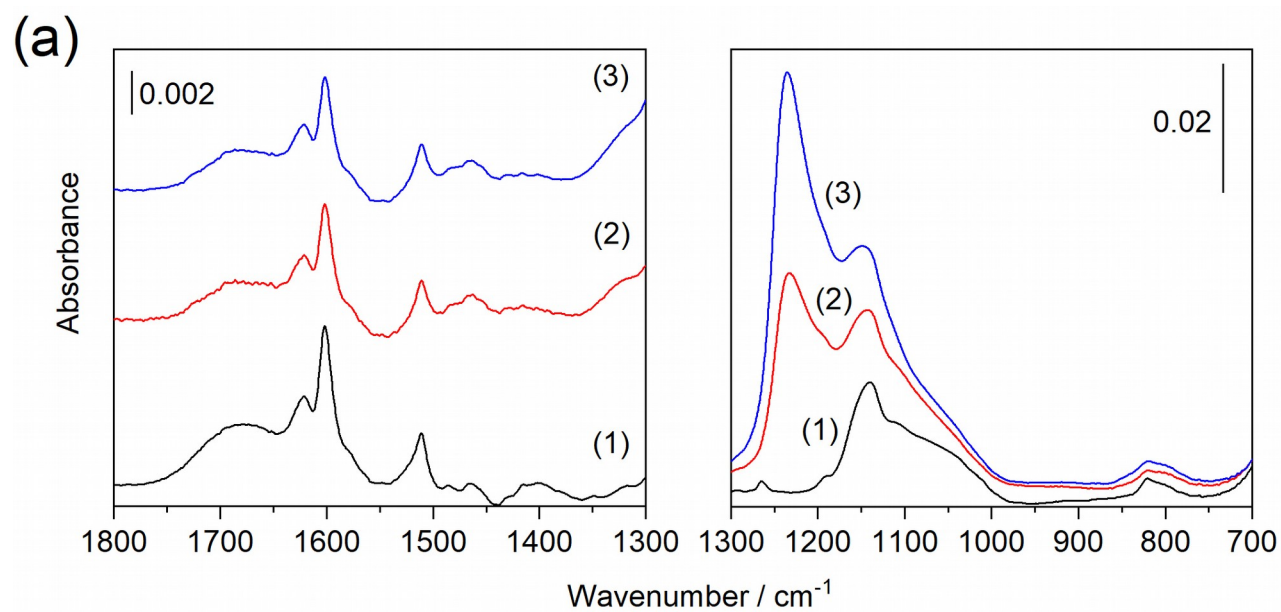


Figure 7: IRRAS of PV3 molecular wire attached to TMSA anchor on Co_3O_4 surface after embedding in silica by ALD. (a) Pt- Co_3O_4 -TMSA-PV3 before silica ALD (trace 1), after 20 cycles SiO_2 ALD (trace 2), and after additional 20 cycles SiO_2 ALD (trace 3). Note that different absorbance scales are used for spectral regions above and below 1300 cm^{-1} . Pt- Co_3O_4 background was subtracted. (b)

TOC Graphics

